Danielle Lopes da Silva

# Imaging the United States through Rayleigh Waves Amplitudes

Niteroi

2023

Danielle Lopes da Silva

# Imaging the United States through Rayleigh Waves Amplitudes

Master Thesis presented to the Graduate Program of Ocean and Earth Dynamics of the Universidade Federal Fluminense as a partial requirement to obtain the degree of master in Geophysics

Universidade Federal Fluminense

Graduate Program of Ocean and Earth Dynamics: Geophysics

Supervisor : William Menke (External)
and Luiz Gamboa (Internal)

Niteroi
2023

Danielle Lopes da Silva

# IMAGING THE UNITED STATES THROUGH RAYLEIGH WAVES AMPLITUDES

Master thesis presented to the Ocean and Earth dynamics graduate program of Universidade Federal Fluminense as a partial requirement for getting the degree of master. Area of focus: Geophysics.

Approved in November of 2023.

EXAMINERS:

---

Prof. William Menke - External Advisor, Columbia University

---

Prof. Luiz Gamboa - Internal Advisor, Universidade Federal Fluminense

---

Prof. Cleverson Guizan Silva, Universidade Federal Fluminense

---

Prof. Sidney Luiz de Matos Mello, Universidade Federal Fluminense

---

Prof. George Sand Leão Araújo de França, Universidade de Brasília

Niterói
2023

Ficha catalográfica automática - SDC/BIG
Gerada com informações fornecidas pelo autor

D111i Da Silva, Danielle Lopes
Imaging the United States through Rayleigh Waves Amplitudes / Danielle Lopes Da Silva. - 2023.
43 f.

Orientador: Luiz Antônio Pierantoni Gambôa.
Coorientador: William H. Menke.
Dissertação (mestrado)-Universidade Federal Fluminense, Instituto de Geociências, Niterói, 2023.

1. Earth Solids. 2. Seismic waves amplitudes. 3. Seismic Attenuation. 4. Produção intelectual. I. Gambôa, Luiz Antônio Pierantoni, orientador. II. Menke, William H., coorientador. III. Universidade Federal Fluminense. Instituto de Geociências. IV. Título.

CDD - XXX

Bibliotecário responsável: Debora do Nascimento - CRB7/6368

*I dedicate this work to all masters I have ever had.*

# Acknowledgements

In that thesis, first of anyone I would like to thank my dear advisor Bill. I met Bill in 2016, when I was still an undergraduate student looking for an opportunity to participate of the Lamont-Doherty Earth Observatory at Columbia University. At the time, Bill believed in me and put a great effort on our work during the summer. After that, Bill was my advisor for my senior thesis. And then, four years later, in 2020, Bill put his faith on me once again, accepting to be my advisor for this work. I cannot find enough words to thank Bill. His effort and beliefs in our work together gave me enough strength to pursue this work, it made me admire him not only as my advisor, but as a kind and caring person. During pandemics, I felt great pleasure in dedicating my time on researching and working on this thesis.

I would not be writing this thesis if Luiz Gamboa, my internal advisor was not supportive as he was. I called him last year, still during the pandemics and he believed in my words when I said I would do my best with this opportunity. He gave me this opportunity and allow me to develop this work. He was always very encouraging on my work and gave very important tips. Thanks for putting your faith and time on me.

I thank my brother Rafael, who still thinks I am the smartest person in the world. My best example of what a man and a father should be. If it was not for him, I would never go to United States and had all the opportunities that put me in this path.

Last but nor least, I thank this work for my partner in life and best friend Carol. Who was always there for my during all times I had to dedicate for work and this thesis. And also for understanding what is like to be married with a scientist.

# Abstract

Surface waves amplitudes are an underutilized source of information about Earth structure. The amplitudes of surface waves may vary with different phenomena such as geometrical spreading, frictional attenuation, or local energy conservation, which occur differently in different geology settings. This work explores the potential of imaging the Earth using the amplitudes of Rayleigh waves that travel from central America to beneath the United States. The earthquakes were chosen to be in a certain magnitude and focal depth to control the seismograms signal-to-noise ratio. Here we show a developed method, able to retrieve seismograms recorded by transportable array stations on IRIS database, process the seismograms and make amplitude analysis depending on frequency and distance from the earthquake focal point. The surface waves amplitudes are able to produce spectral amplitude maps and inverse Q factor maps that correlate with geological structure and that have coherency for different surface waves periods. The resulting spectral amplitude maps from this work compliment velocity maps done using surface waves and body waves from previous works and the amplitude decay plots infer quality factor values that are consistent with the different geology setting of the United States.

Key words: Surface waves; Attenuation; Seismic waves amplitudes;

# Resumo

As amplitudes das ondas de superfície são uma fonte subutilizada de informações sobre a estrutura da Terra. As amplitudes das ondas de superfície podem variar com diferentes fenômenos, como espalhamento geométrico, atenuação por atrito ou conservação de energia local, que ocorrem de maneira diferente em diferentes configurações geológicas. Este trabalho explora o potencial de imageamento da Terra usando as amplitudes das ondas Rayleigh que viajam da América Central até os Estados Unidos. Os terremotos foram escolhidos para ter uma certa magnitude e profundidade focal para controlar a relação sinal-ruído dos sismogramas. Aqui mostramos um método desenvolvido, capaz de recuperar sismogramas gravados no banco de dados IRIS, processar os sismogramas e fazer análises de amplitude dependendo da frequência e distância do ponto focal do terremoto. As amplitudes das ondas de superfície são capazes de produzir mapas de amplitude espectral e mapas de fator Q inverso que se correlacionam com a estrutura geológica e que possuem coerência para diferentes períodos de ondas de superfície. Os mapas de amplitude espectral resultantes deste trabalho complementam os mapas de velocidade feitos usando ondas de superfície e ondas de corpo de trabalhos anteriores e os gráficos de decaimento de amplitude inferem valores de fator de qualidade que são consistentes com diferentes configurações geológicas dos Estados Unidos.

Palavras-chave: Ondas de superfície; Atenuação; Amplitude sísmica;

*"Failure is an important part of your growth and developing resilience. Don't be afraid to fail."*

Michelle Obama

# List of Figures

# Contents

# 1 Introduction

## 1.1 Geology Overview

The United States is a wide country that contains several regions, which differ in their geological history and tectonic setting. The continental United States is set inside the North American plate, which is bounded on the west by a complex system of faults, such as the very well known San Andreas fault of California and the Cascadia subduction zone, and on the east by mid-Atlantic ridge. The North American plate is moving west-southwest with rate about 2.5 cm/yr, relative to the lower mantle (KREEMER, 2009). The Pacific plate moves northwest relative to North America at a rate of about 6cm/yr, sliding along the San Andreas and other transform faults, to be subducted beneath southern Alaska and the Aleutian chain(PAKISER; MOONEY, 1989). Offshore Oregon and Washington, two small oceanic plates, the Gorda and Juan de Fuca Plate, lie between the Pacific and North American plates. It is being subducted beneath North America along the Cascadia subduction zone (Figure 1).

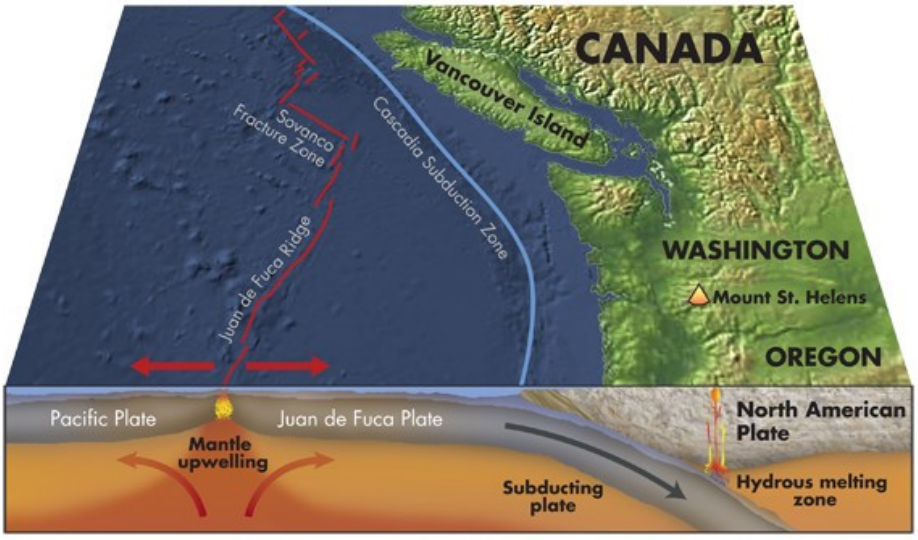


Figure 1 – The Cascadia Subduction Zone is a 1,000-kilometer-long subduction zone stretching from Mendocino, California, to north of Vancouver Island off the coast of British Columbia. It is capable of producing magnitude-9-plus earthquakes. (WATTS, 2014)

The continental margin of the western North America is considered as an active margin characterized by two plate tectonic styles: strike slip faulting and convergence (COUCH; RIDDIHOUGH, 1989). Extreme western of the US has been shaped by the arc volcanism associated to the now-defunct subduction of the Farallon oceanic plate beneath

California, and the present-day subduction of the Gorda and Juan de Fuca oceanic plates beneath Oregin and Washington. This region included the Mesozoic batholith of the Sierra Nevada Mountains in California and the active Cascade volcanoes in Oregon Washington (figure 2).

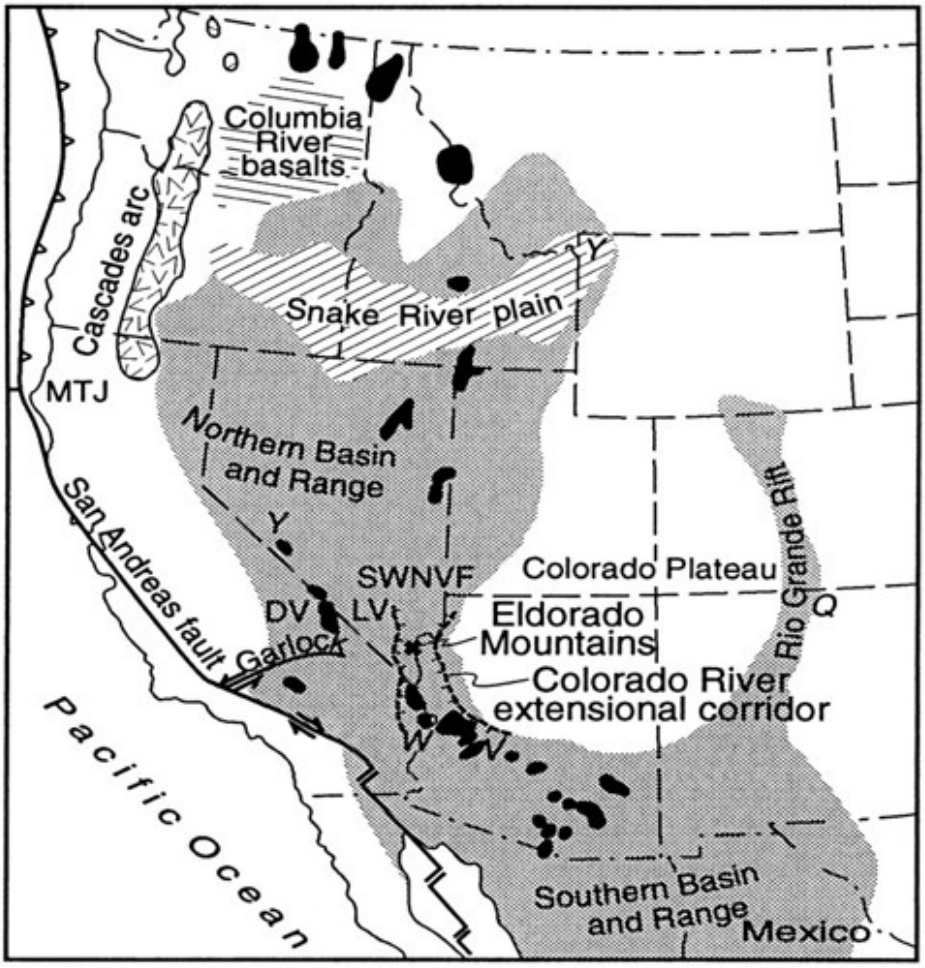


Figure 2 – Basin and range extension along the western part of United States.(GANS; BOHRSON, 1998)

The Basin and Range province is characterized by extensional fault-block mountains and deep, sediment-filled basins. In the states of Nevada and Utah the province lies between the uplifted blocks of the Sierra Nevada on the west and the Colorado Plateau to join the Rio Grande rift (PAKISER; MOONEY, 1989). During Cenozoic time the northern Basin and Range province has widened about 250km by the motion of the Sierra Nevada (FREI, 1986). This extension is marked by features like widespread seismicity, fault scarps and intrusive and extrusive igneous activity. In addition, the crust is thin (about 35km or less) and the upper mantle P-wave velocities reported are low (PAKISER; MOONEY, 1989), implying that the mantle lithosphere is very thin as well. The heat flow increases and causes low mantle velocities. These delays of S-waves are interpreted as partial melting in the upper mantle (ROMANOWICZ, 1979).

In contrast to the western North America, the eastern part is a cratonic, and experiencing very little present-day tectonic activity. The crust is thick (up to 50km) (ABBOTT; MOONEY, 1995) and upper mantle seismic velocities are high, implying a thick mantle lithosphere. In works such as (SCHMANDT; LIN, 2014) is very obvious to see the overall high velocities the eastern US.

Another major feature in North America is the Paleozoic mountain chain, the Appalachians. The present mountains result from Tertiary uplift of dissected Mesozoic and Tertiary surfaces as the crust readjusted isostatically to erosional unloading (HATCHER ROBERT D.; THOMAS; VIELE, 1989).

Some of the contacts of these main structural features of United States can be seen in the figure 3.

Geophysical indirect measurements are able to detect the different provinces in North America. Surface waves amplitudes are an underutilized source of information about the Earth's structure. It is known that different geology setting can lead to distinct physical phenomena, such as geometrical spreading, attenuation and local energy conservation, that may affect amplitude information. In this work, we expect to explore the imaging potential of surface seismic waves amplitude variation in United States. The next chapters will give a summary of the overall knowledge necessary to comprehend the fundamentals and the methods behind this study.

## 1.2 Objectives of this thesis

I - Using Rayleigh waves as input, to develop PYTHON scripts able to process and organize all data retrieved.

II - To develop a processing PYTHON scripts to be able process the seismograms, get the Rayleigh waves from them and compute amplitude spectral data maps along all Unites States for different frequency bands.

III - Interpret major structures seen in the amplitude spectral maps and inverse Q maps for different frequency bands and associate them with structure from different depths.

IV - Compare the results of the produced maps with previous works.

V - Discuss the physical mechanisms that could explain the results seem in the Spectral Amplitude maps such as spherical spreading, intrinsic attenuation and local velocity variation.

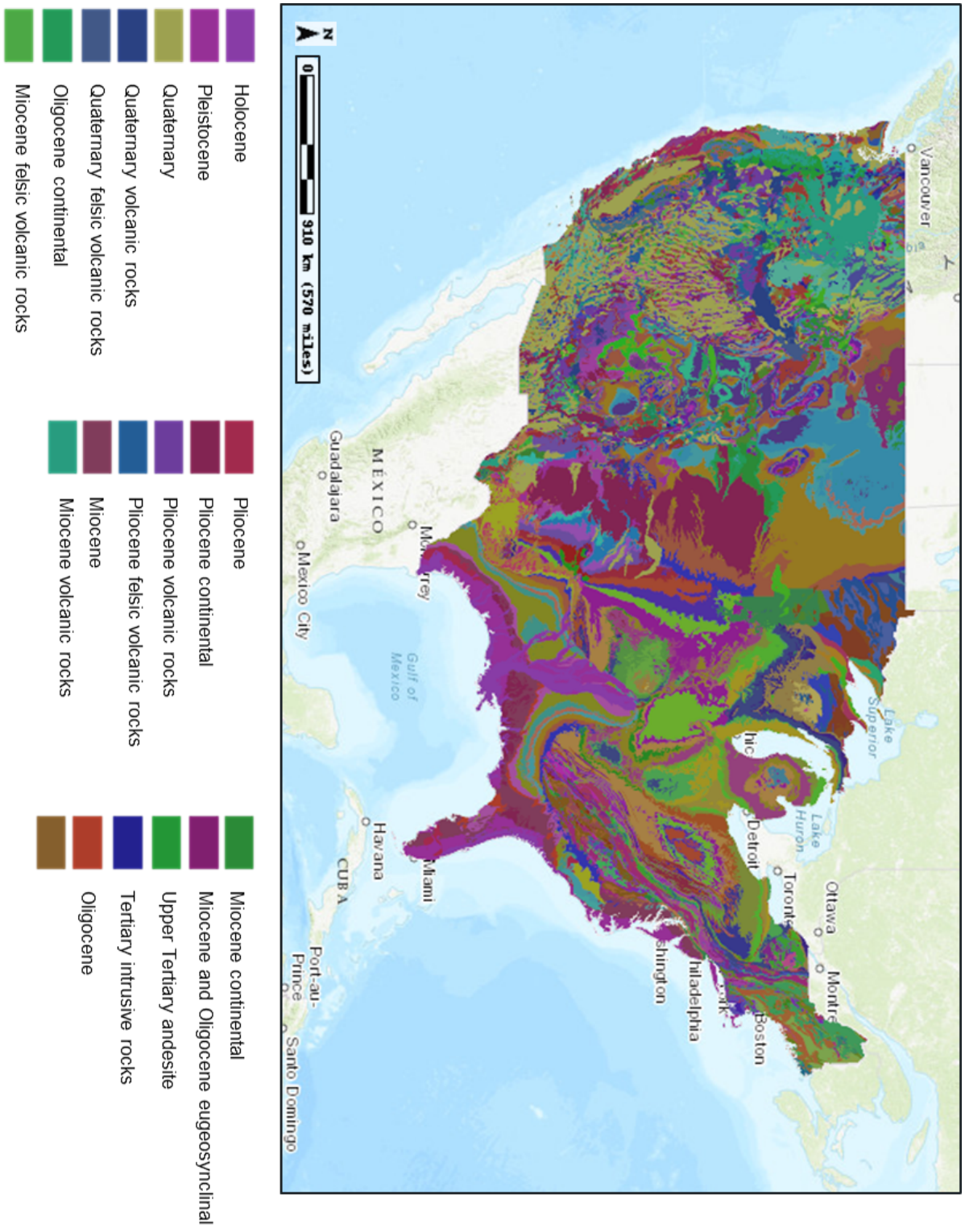


Figure 3 – Geological map of United states showing the major features of the country. (ARNDT WALTER J. BAWIEC, 1994)

# 2 Basics of Seismology

Seismology is known as the science that studies the waves produced by earthquakes and what they tell us about Earth's deep interior, where direct observations are impossible (SHEARER, 2019). Seismology is a very important field of Earth Sciences, it is related to understanding the physical processes that cause earthquakes and also reducing the impacts of them in humanity. It presents theoretical issues such as the propagation of elastic waves and inversion of geophysical data, topics that will be treated next in this work.

Although seismology is a young science (about 100 years), the applications of it extend from studying the Earth core to evaluate hydrocarbon deposits under a thick layer of salt. Driven by the observation that usually volcanos and earthquakes were related, works started to be developed by Cauchy, Poisson, Stokes, Rayleigh and others to describe the wave propagation physics and the different kinds of wave known at that time, such as compressional waves (also called primary or P waves)and shear waves (also called secondary or S waves).

## 2.1 Seismic Waves

With the advance of technology the seismic instrumentation developed from undamped pendulums to seismometers, able to record during the entire duration of earthquakes. The seismograms, signals recorded by the seismometers, allow a fast progress in determining Earth's seismic velocity structure. Around 1830, Poisson, using the elastic laws and equations of motion, showed that two fundamental kinds of waves propagate in homogeneous solids, which are P waves (compressional) na S waves. P waves, also called Primary, are compressional waves involving volumetric disturbances, such as sound waves. S waves, also called Secondary, present only shear deformation, with no change in volume and do not propagate in fluids. Those waves are called body waves, once they traverse the interior of the medium. P waves travel faster than S waves.

Rayleigh, in 1887, demonstrated the presence of additional kinds of waves, which are also solutions of elastic equations. These are called Rayleigh waves, involving wave motions confined to and propagating along the surface of the body. Rayleigh waves are a type of surface wave that propagate near the Earth's surface as ripples and cause a rotation that can be either prograde (along the direction of propagation) or retrograde (against the direction of propagation). They are also called ground roll due to the nature of their movement (J.; A.; E., 2019). Around 1911, the Love waves were characterized, a second type of surface waves. They travel orthogonaly with the direction of propagation but parallel with the surface of the Earth. Surface waves are result from the interaction

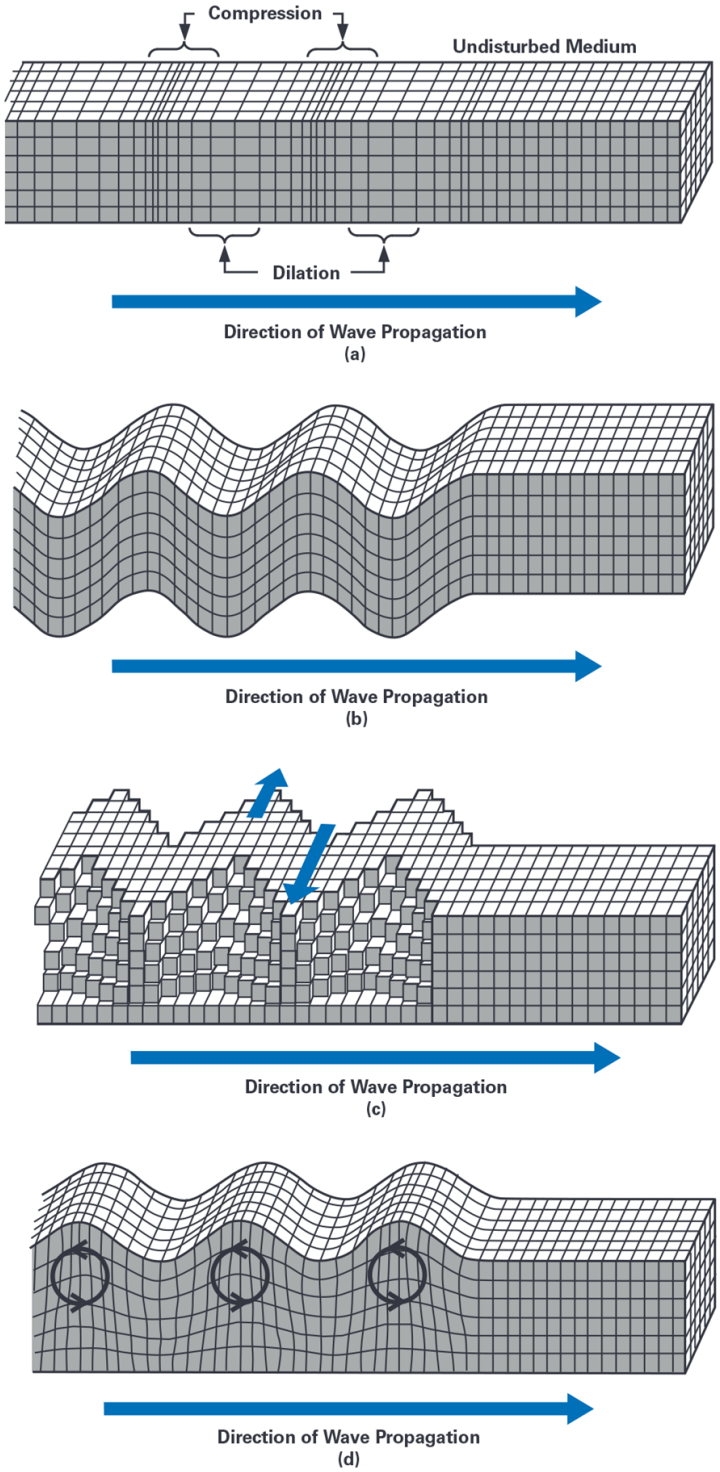


Figure 4 – Types of seismic waves: (a) primary waves; (b) secondary waves; (c) Love waves; (d) Rayleigh waves (J.; A.; E., 2019)

of P and S waves with the boundary conditions of the body (LAY; WALLACE, 1995). Figure 5 shows the behavior of particle motion for body and surface waves.

The physics that describes the propagation of seismic waves is based on Newton's second law of motion

$$F = ma \tag{2.1}$$

where $F$ is the applied force, $m$ is the mass and $a$ the acceleration. For a continuous medium equation 2.1 becomes

$$\rho \frac{\partial^2 u_i}{\partial t^2} = \frac{\partial \tau_{ij}}{\partial j} + f_i \tag{2.2}$$

where $p$ is the density, $u$ is the displacement and $\tau$ is the stress tensor. This is called the momentum equation or the equation of motion. The body force term $f$ generally consists of a gravity term $f_g$ and a source term $f_s$. Gravity is an important factor at very low frequencies in normal mode seismology, but it can generally be neglected for body- and surface-wave calculations at typically observed wavelengths. In the absence of body forces, we have the homogeneous equation of motion which governs seismic wave propagation outside of seismic source regions (SHEARER, 2019). In order to solve 2.2 we require a relationship between stress and strain so that we can express $\tau$ in terms of the displacement $u$. Because strains associated with seismic waves are generally very small, we can assume a linear stress-strain relationship and write the stress as a function of strain and the Lame parameters $\lambda$ and $\mu$

$$\tau_{ij} = \lambda \delta_{ij} \epsilon_{kk} + 2\mu \epsilon_{ij} \tag{2.3}$$

where $\epsilon$ is the strain tensor. After a series of substitutions it is possible o separate the equation into P wave equation and S wave equation. From that, P velocity is written as

$$v_p = \sqrt{\frac{\lambda + 2\mu}{\rho}} \tag{2.4}$$

and S velocity is written as

$$v_s = \sqrt{\frac{\mu}{\rho}} \tag{2.5}$$

where $\mu$ and $\lambda$ are bulk and shear moduli.

Primary waves have speed around 5km/s to 8km/s. they are the least destructive type of wave due to their fast energy decay. S-waves have velocities around 60% and 70% of the P waves. They are more destructive than P waves, once their energy decay is lower. Surface waves are 10% slower than body waves, but they are the most destructive. It is worth noting that the propagation velocity of seismic waves varies widely depending on

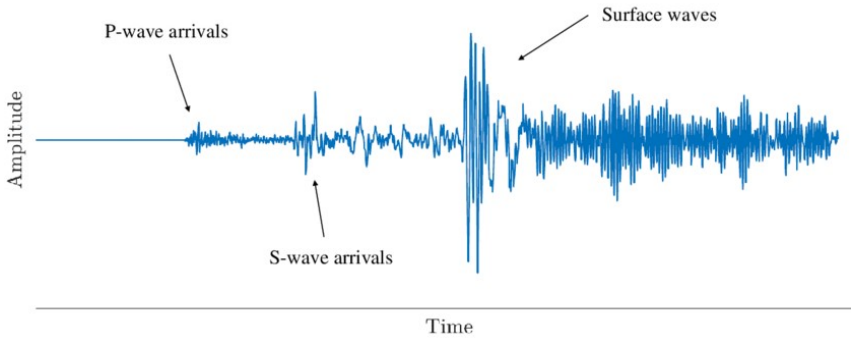


Figure 5 – The seismogram shows the arrival times and amplitudes of ground motion for P, S and Surface waves (HOHENSINN, 2019)

the type of soil they are traveling in. Figure 5 shows an example of seismogram, showing the arrival times and ampliude of ground motion for body and surface waves.

## 2.2 Earth Structure

Seismic wave velocities are strongly related to the medium of propagation, and therefore, to the geology set. As saw on equations 2.4 and 2.5 the body wave velocities are affected by the Lamé parameters $\lambda$ and $\mu$, also called bulk and shear module, respectively. In materials science the Lamé parameters quantify the stress-strain relationship, as the ratio of an applied force and the deformation created by it. As expected, those parameters are intrinsic to the material. Figure 6 shows a list of different materials and the average seismic velocities.

| Material | Seismic Velocity (m/sec) |
|---|---|
| Loose and dry soils | 182.880-1005.840 |
| Clay and wet soils | 762.000-1920.240 |
| Coarse and compact soils | 914.400-2590.800 |
| Sandstone and cemented soils | 914.400-4267.200 |
| Shale and marl | 1828.800-5334.000 |
| Limestone-chalk | 2133.600-6400.800 |
| Metamorphic rocks | 3048.000-6400.800 |
| Volcanic rocks | 3048.000-6858.000 |
| Sound plutonic rocks | 3962.400-7620.000 |
| Jointed granite | 243.840-4572.000 |
| Weathered rocks | 609.600-3048.000 |

Figure 6 – List of different materials and their average seismic propagation velocities (HACıEFENDIOğLU et al., 2015)

The study of the seismic waves and observations on seismograms lead to conclusions about the Earth composition. Richard Oldham was the one to detected the presence of Earth's core from the absence of direct P and S arrivals at source-receiver distances beyond about 100 degrees. Andrija Mohorovičić in 1909 reported observations showing

the existence of a velocity discontinuity separating crust and mantle (SHEARER, 2019). Many authors started to produce their velocity-depth variation tables from the travel times observed in the seismograms.

The ocean crust is estimated to be about 6km wide whereas the continental crust is about 30-50km wide. Besides the crust, the Earths interior can be divided in layers such as the mantle, outer core and inner core. The mantle represents about 84 % of the Earth. It is marked by a fast velocity in the upper mantle (300 - 700km depth, also called transition zone) where various mineralogical changes occur. From 700km depth to core mantle boundary (CMB) the velocities increase in agreement with changes in the pressure and temperature. Whereas at the CMB the P velocity drops from about 14km/s to 8km/s due to the interface between the mantle and the fluid outer core. The Earth's core is believed to be composed by iron and the inner-core boundary (ICB) is thought to represent a phase change in iron to a different crystal structure (SHEARER, 2019). Figure 7 shows velocity and density profiles for different depths.

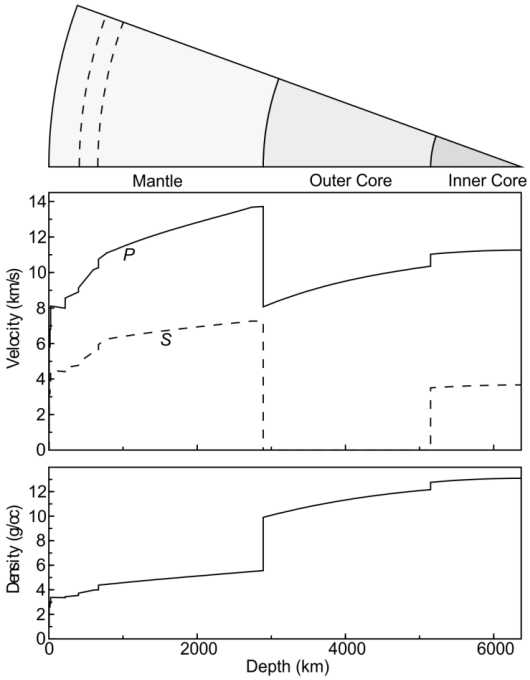


Figure 7 – Earth's P velocity, S velocity, and density as a function of depth. Values are plotted from the Preliminary Reference Earth Model (PREM) of DZIEWONSKI; ANDERSON (1981); except for some differences in the upper mantle, all modern Earth models are close to these values (SHEARER, 2019).

# 3 Imaging United States using Surface Waves Amplitudes

Brazilian Journal of Geophysics
Brazilian Geophysical Society
ISSN 0102-261X

## Imaging United States using Surface Waves Amplitudes

Earth Solids; Rayleigh waves; Spectral Analysis

Abstract

Surface waves amplitudes are an underutilized source of information about Earth structure. The amplitudes of surface waves may vary with different phenomena such as geometrical spreading, frictional attenuation, or local energy conservation, which occur differently in different geology settings. This work explores the potential of imaging the Earth using the amplitudes of Rayleigh waves that travel from central America to beneath the United States. The earthquakes were chosen to be in a certain magnitude and focal depth to control the seismograms signal-to-noise ratio. Here we show a developed method, able to retrieve seismograms recorded by transportable array stations on IRIS database, process the seismograms and make amplitude analysis depending on frequency and distance from the earthquake focal point. The surface waves amplitudes are able to produce spectral amplitude maps that correlate with geological structure and that have coherency for different surface waves periods. The resulting spectral amplitude maps from this work compliment velocity maps done using surface waves and body waves from previous works and the amplitude decay plots infer quality factor values that are consistent with the different geology setting of the United States.

## INTRODUCTION

This work explores the imaging power of the amplitude variation of surface waves traveling across the Earth. Physical considerations suggest that phenomena such as geometrical spreading, frictional attenuation, and local energy conservation affect surface waves amplitudes. In this work, the physical phenomena are used to justify this amplitude

variation and to infer about physical proprieties on the study area, such as the quality factor, Q. When surface waves travel along the Earth, their amplitudes tend to decrease with the distance from source, because, to conserve energy, amplitude must decrease as the radius of the wave front grows larger. This effect is called circular spreading and can be expressed as:

$$A(x) = A_0/\sqrt{x} \tag{3.1}$$

where $A(x)$ is the amplitude on distance $x$ and $A_0$ is the initial amplitude when $x = 1$. Geometrical spreading also operates on smaller scale due to the lensing effect. Here, a small patch of low velocities causes ray paths to converge, leading to focusing and higher amplitudes, and a small patch of high velocities cause rays to diverge, leading to defocusing and lower amplitudes. Circular spreading is not always sufficient to explain the amplitude variations observed in seismic data. The frictional attenuation is needed to explain the decay of amplitude in some geology settings. The quality factor, Q, is a dimensionless parameter that quantifies the intrinsic amplitude attenuation and velocity dispersion in inelastic mediums. Different materials have different Q factors, leading waves to be attenuated differently in each of them. This amplitude variation can be expressed as:

$$A(x) = A_0 e^{-\alpha x} \tag{3.2}$$

where *alpha* is the attenuation factor. It is related to the Q factor by the equation:

$$\alpha = \pi f/Qc \tag{3.3}$$

where $f$ and $c$ are the frequency and the velocity of the wave in the medium.

Local energy conservation also is expected to lead to lateral variations in amplitude, because energy density is proportional to the product of velocity and amplitude squared. When waves travel from a low velocity zone to a high velocity zone, their amplitude decreases to offset their increased velocity. The stiffness of a high velocity material enables it to store the same energy with less amplitude of motion. This can be described by the equation

$$c_0 A_0^2 = c_1 A_1^2$$

or

$$A_1 = A_0 \sqrt{\frac{c_0}{c_1}} \tag{3.4}$$

where $c_0$ and $c_1$ are the velocities for different materials. The amplitude variations caused by the phenomena described above will affect the amplitude observations for surface waves travelling through different geology.

## The Study Area

The United States is a large country that contains several regions that differ in their geological history and tectonic setting. The continental United States is set inside the North American plate, which is bounded on the west by a complex system of faults, such as the very well-known San Andreas fault of California and the Cascadia subduction zone, and on the east by mid-Atlantic ridge. The North American plate is moving west-southwest with rate about 2.5 cm/yr, relative to the lower mantle (KREEMER, 2009). The Pacific plate moves northwest relative to North America at a rate of about 6 cm/yr, sliding along the San Andreas and other transform faults, to be subducted beneath southern Alaska and the Aleutian chain(PAKISER; MOONEY, 1989). Offshore Oregon and Washington, two small oceanic plates, Gorda and Juan de Fuca, lie between the Pacific and North American plates. They are being subducted beneath North America along the Cascadia subduction zone.

Extreme western of the US has been shaped by the arc volcanism associated to the now-defunct subduction of the Farallon oceanic plate beneath California, and the present-day subduction of the Gorda and Juan de Fuca oceanic plates beneath Oregon and Washington. This region includes the Mesozoic batholith of the Sierra Nevada Mountains in California and the active Cascade volcanoes in Oregon Washington. The Basin and Range province is characterized by extensional fault-block mountains and deep, sediment-filled basins. During Cenozoic time the northern Basin and Range province has widened about 250km by the motion of the Sierra Nevada (FREI, 1986). This extension is marked by features like widespread seismicity, fault scarps and intrusive and extrusive igneous activity. In addition, it led to the region's thin crust (about 35 km or less) and elevated head flow. Upper mantle P-wave velocities are low (PAKISER; MOONEY, 1989), implying that the mantle lithosphere is very thin as well. Low S velocities in the upper mantle are interpreted as due to partial melting in the asthenosphere (ROMANOWICZ, 1979).

In contrast to the western North America, the eastern part is cratonic and is experiencing very little present-day tectonic activity. The crust is thick (up to 50km) (Abbott and Mooney, 1995) and upper mantle seismic velocities are high, implying a thick mantle lithosphere. The high velocities of the craton are very clearly visible in continent scale tomographic images (SCHMANDT; LIN, 2014). A major feature in eastern North America is the Paleozoic Appalachian Mountain belt. The present mountains result from Tertiary uplift of dissected Mesozoic and Tertiary surfaces as the crust readjusted isostatically to erosional unloading (HATCHER ROBERT D., 1989). Some of the contacts

of these main structural features of the United States can be seen in the figure 8. Geophysical indirect measurements are able to detect the different provinces in North America.

In this work, surface seismic waves propagation is used in order to understand how it can contribute in the study of the United States subsurface structure and geology.

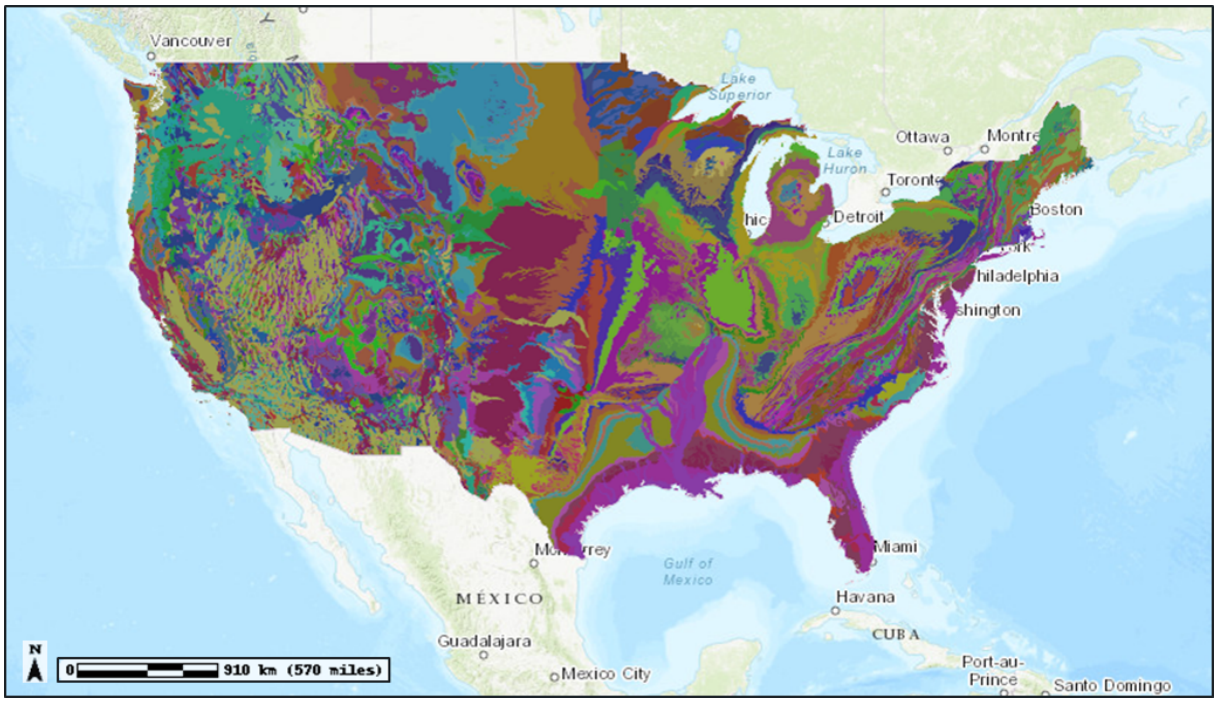


Figure 8 – The geological map of the United States shows the main tectonic and lithologic provinces of the country. It is possible to see the contrast of deposits on the craton to the deposits on active margin and orogenic belts. (ARNDT WALTER J. BAWIEC, 1994)

# METHODS

A large number of high-quality seismic recording stations is essential for studying seismic waves propagation. In an international context, United States is in a good study area, with hundreds of stations distributed throughout its territory, including Transportable Array stations. The Transportable Array is composed by 400 seismic stations that traversed all conterminous United States during a seven-year-long project (2007-2013) occupying a total of two thousand sites each for about eighteen months (Fig. 14). The seismometers have three-component broadband geophones recorded with a sample rate of the stations is about 40 samples/second, enabling excellent recordings of both low and high frequency seismic waves. Station spacing is about 70 km. The Transportable Array is very useful for mapping the structure of the Earth beneath United States using seismic waves from earthquakes because it can record even small earthquakes. However, the movement of the TA stations preclude making synoptic measurements; any given earthquake is observed

only on a "slice" through the array. Transportable Array data is archived by IRIS Data Management Center and is publicly available for studies such as this current work.

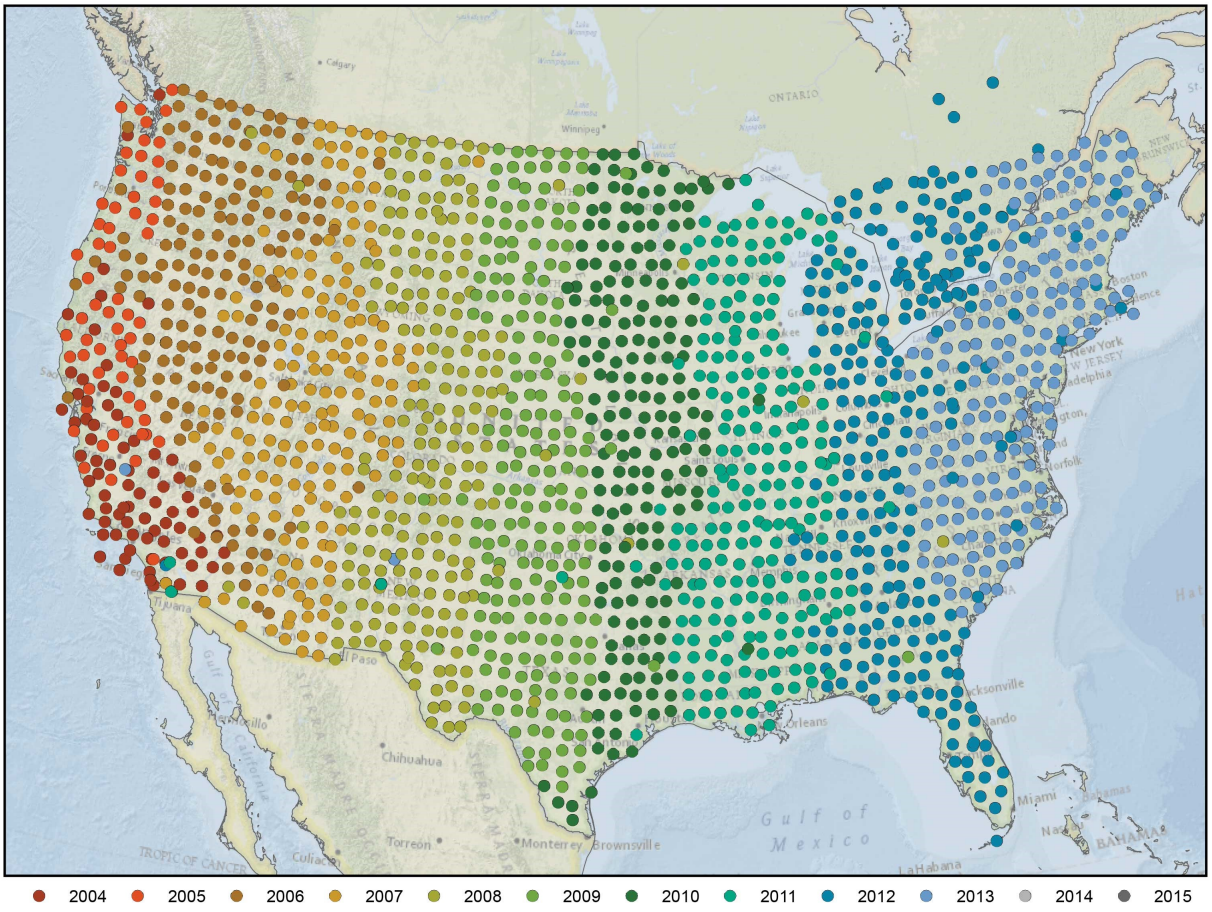


Figure 9 – Distribution of Transportable Array Stations along United Stated along the past decade. Source: Earthscope.

## Database

In order that any given earthquake be recorded over the widest distance range, we focused on waves that propagated north-south, along the long-axis of TA slices. Few earthquakes occur to the north of conterminous US, so the study was limited to earthquakes from the south. These earthquakes occurred along the Central America plate tectonics margin, mainly at the Cocos plate and North American, Caribbean and Panama plates boundaries. Only earthquakes with magnitudes in the 6.5 to 7.5 range with and depth less than 50km (suitable focal depth for excite for surface waves) are used (Fig. 10). Earthquake hypocentral parameters are taken from USGS Earthquake catalog. one for each year in the Central America area. The database consists of nine earthquakes (about one per year). TA stations operating at the time of a given earthquake were determined using IRIS Stations Inventories webpage and seismogram data were obtained using IRIS BREQ FAST data retrieval service. The downloaded data was in MiniSEED format. MiniSEED is a

stripped-down version of Standard for the Exchange of Earthquake Data (SEED) format, an international standard for the archival and exchange of seismological time series data and related metadata.

a)

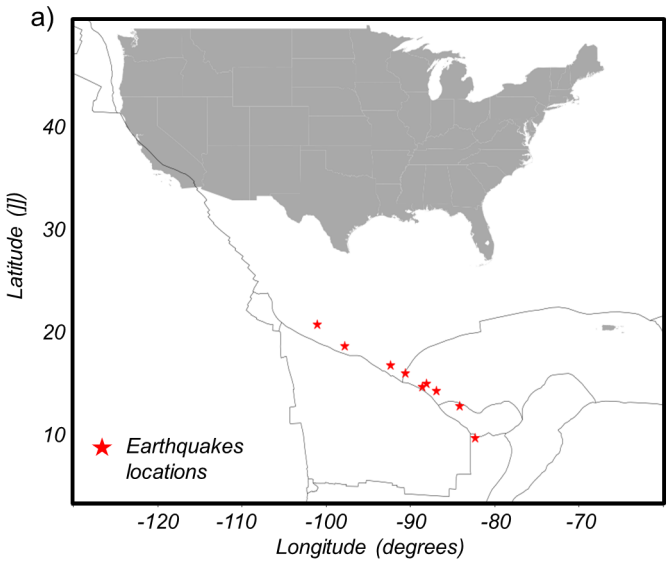


b)

| year | magnitude | Focal depth(km) | Lat | Lon |
|---|---|---|---|---|
| 2006 | 6.1 | 56.0 | 18.5N | 90.6W |
| 2007 | 6.7 | 23.0 | 13.5N | 90.6W |
| 2008 | 6.7 | 24.0 | 14.4N | 92.3W |
| 2009 | 6.1 | 14.0 | 10.2N | 84.2W |
| 2010 | 6.3 | 20.0 | 16.4N | 97.8W |
| 2011 | 6.1 | 12.0 | 6.8N | 82.3W |
| 2012 | 7.3 | 28.0 | 12.1N | 88.5W |
| 2013 | 6.5 | 30.0 | 11.7N | 86.9W |
| 2014 | 7.3 | 30.0 | 12.5N | 88.1W |

Figure 10 – : (a) Earthquakes locations are marked in the map as red starts; (2) Location, date, focal depth, and magnitudes for each earthquake used in this study.

## Data Processing

The following data processing steps were performed for each set of stations for each earthquake used in the analysis.

1. Interpolation to time base starting at earthquake origin start time. In this step the data is interpolated to a common time base with sample 0 being at the origin time of the event. A rate of 100 samples per second is used, which is the highest typically recorded by any of the stations we used. 2. Correction for instrument response to displacement. Correcting the instrument response factor is crucial to have a reliable information in the data analysis waveform amplitudes, because several different model seismometers with different sensitivities and frequency responses are used at TA stations. IRIS RESP files containing response information were obtained for each from the IRIS Website. A RESP file is an ASCII representation of the response information. By removing the instrument response, the seismogram is changed from units of digital counts to units of displacement in meters. 3. Rotation to (Z,R,T) coordinates, which isolates the Rayleigh wave on the (Z,R) components. 4. Archiving the processed seismograms, along with metadata such as station and event locations in a Python-readable Pickle file. Each earthquake-station pair was stores in a separated file.

## Amplitude computation

Spectral amplitude was computed for each station recording a given event following the steps:

1. Choice of components. The vertical component was chosen as the one appropriate for measuring Rayleigh wave amplitudes, because it usually has the highest signal-to-noise ratio.

2. Windowing of seismograms. Seismograms are windowed to isolate to a time interval that included mostly Rayleigh waves starting time, $t_{wstart}$, and end time, $t_{wend}$, of the window were adjusted according to the earthquake-station distance. The time, $t_{wstart}$, was small enough to include the longest period Rayleigh waves, that travel at about 4.5k m/s. The time, $t_{wend}$, was chosen manually, by examining the station was the most far from the earthquake, and ensuring that the short periods Rayleigh waves, whose generally slow velocities depend strongly on crustal structure, within the window. A standard Hamming taper was applied to the windowed data in order to reduce artifacts that occur during spectral analysis.

3. Calculation of Spectra. Once the seismograms are windowed, the spectral amplitude was computed using standard Fourier analysis.

4. Averaging in pre-determined bands. The average of the spectral amplitude was computed for four frequency bands, 0.02 to 0.065 Hz, 0.065 to 0.11 Hz, 0.11 to 0.155 Hz and 0.155 to 0.2 Hz. As the depth sensitivity of Rayleigh waves is known to decrease with periods, amplitude maps the different bands has different target depth. Thus, amplitude information for given earthquake-station pair is summarized by four average amplitude values.

## Post processing and Amplitude Normalization

Amplitudes for a given earthquake are measured only for a slice through the Transportable Array – the slice that was in operation at the time of the earthquake. In order to connect the slices into a single, continent-spanning map, a correction must be applied to each slice that empirically corrects for differences in earthquake source parameters, such as depth of focus, magnitude, and hypocentral location. The slices can then be combined into an approximately synoptic map. The correction factor can be computed using two different approaches.

1. Calculating the normalization factor for a pair of events at the time using common stations. In this approach, the amplitudes of common stations for events with adjacent slices are compared, and the factor that best equalizes the amplitudes is computed using linear regression. With the slices numbered west to east by the year of the respective earthquake, we adjust slice 2007 to 2006, 2008 to 2007, etc. The 2007 and 2008 slices are

shown as an example (Fig. 11a). The slope of the linear regression is the factor that brings the event from 2008 to the same amplitude level from 2007. The final amplitudes will be similar and comparable, producing a combined, two-slice amplitude map with smooth join between slices.

2. Calculating the normalization factor just once for all events. In this second approach, amplitudes for all events are considered together. Inspecting a plot of amplitudes versus distance (Fig. 11b), it is evident that the amplitude decreases with distance in a non-linear fashion. The relationship between amplitude and distance is assumed to vary according to the empirical relationship

$$A_k i = C_k x_{k_i}^{-\psi} \tag{3.5}$$

Here, events are indexed by k and stations by i. Taking the logarithm of both sides of the equation, 3.5 can be written as

$$log(A_{ki}) = log(C_k x_{k_i}^{-\psi}) = log(C_k) - \psi log(x_{ki}) \tag{3.6}$$

The slope $\psi$ and correction factors, $C_k$, are estimated using a linear regression. The correction factors can then be used to normalize the events to a common amplitude. The slope parameter was found to be  = 0.59. Although both approaches were tested, the second was found to be the better and is the one used in this work.

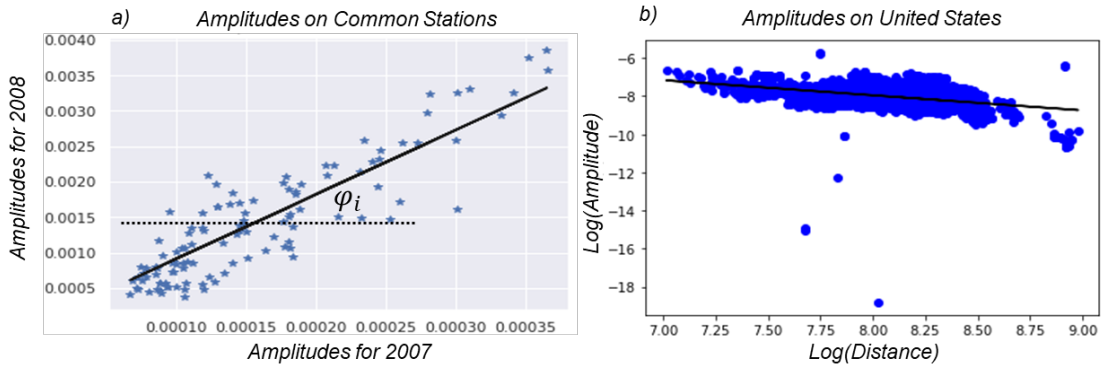


Figure 11 – (a) linear regression is used to infer the slope between amplitude of common stations from different events. (b) amplitudes for all stations are considered in order to find a global slope. As an example, this was done for band from 0.065 to 0.11Hz.

## Python Script

An important part of this work is the computational workflow developed in Python language. The Python scripts were responsible for retrieving, processing and organizing

all the data. In addition, all the analysis and results produced, such as plots and maps, were developed in Python language. Figure 12 summarizes this python workflow.

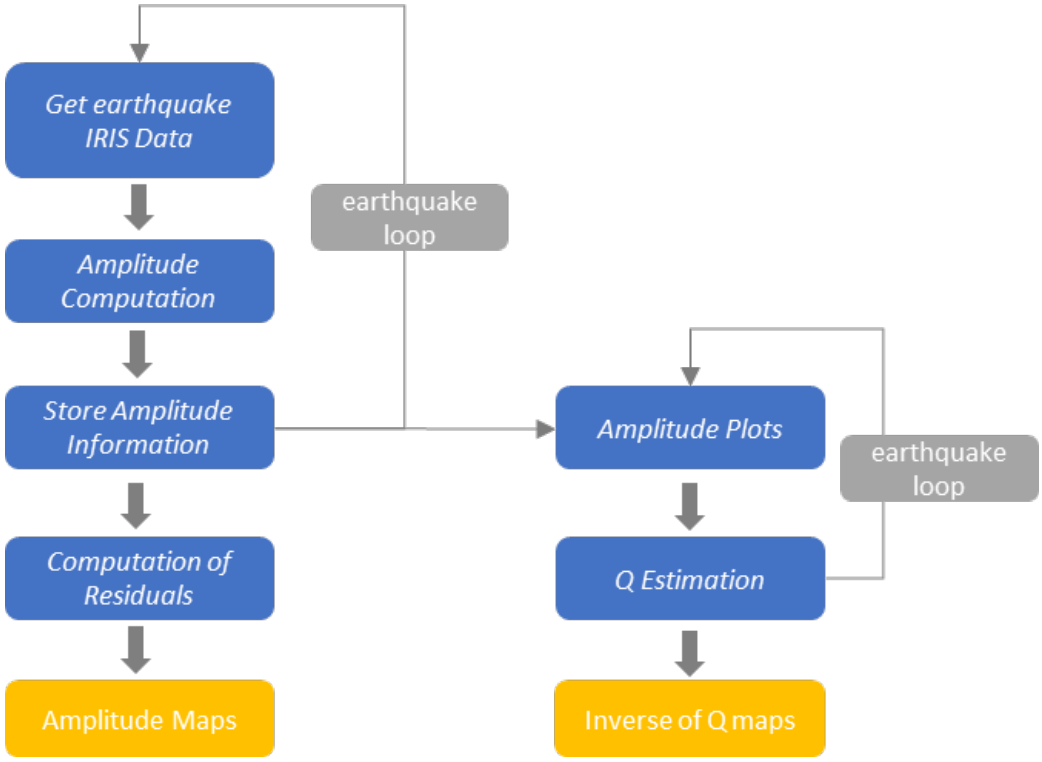


Figure 12 – Python workflow including retrieving, processing and doing all the data analysis.

Figure 13 shows a piece of python code that is responsible for storing the spectral amplitude information into table files. This was one of the scripts that had to be run for all the earthquakes.

```
# part 6  write A and other information to a file


D = np.concatenate( (lat,lon,A), axis=1);
D=pd.DataFrame(D,columns =['Lat', 'Lon',  'B1','B2','B3','B4'])
D['distance'] = ERANGE;
D['station'] = stat;
# write text file containig D

filename="./spec_map/%s_spec.txt" % (eventdir);

D.to_csv(filename, header=None, index=None, sep='\t', mode='a')
```

Figure 13 – Python piece of code responsible for writing spectral amplitude information in a table file together with the stations information.

## Computation of residuals

A plot of amplitudes for an exemplary earthquake (Fig. 14) exhibits a large amount of scatter about a general decline of amplitude with distance. Although a map of the same data (Fig. 14B) depicts this same general decline, it demonstrates that the scatter is not random, but due to spatially-coherent variation in amplitude. In order to increase the resolution of the maps, amplitude residuals were computed (Fig. 14c). Considering that, the residual amplitude $\delta_{ki}$ in station i and event k is defines as

$$\delta_{ki} = log(A_{ki}) - C_k - \psi log(x_{ki}) \tag{3.7}$$

The residual amplitude map on figure 14d) shows more details than does the amplitude map (Fig. 14b). For instance, the linear feature southwest of Arizona in the amplitude map (Fig. 14c) is more clearly extend though the northwest of United States in the amplitude residual map.

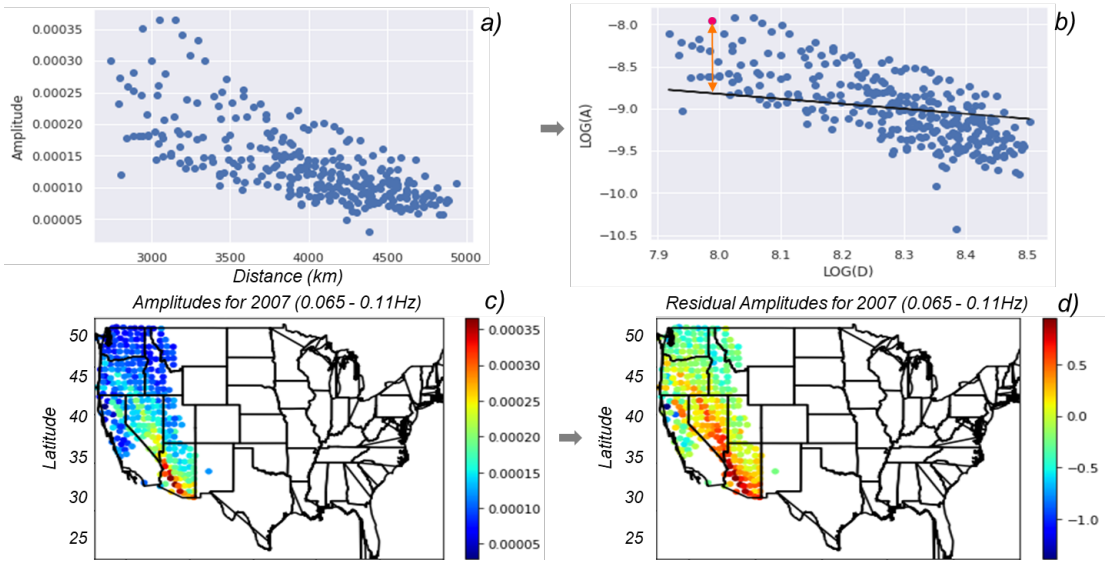


Figure 14 – On a) and b) it is possible to see the amplitude behavior varying with distance and its logarithm, respectively. The orange arrow shows the difference between the expected amplitude calculated considering $(C_k + \psi log x_{ki}))$ and the logarithm of the measured amplitude at same location $(logA_{ki})$, which is defined as the amplitude residual $\delta_{ki}$. Parts c) and d) show the difference between the raw spectral amplitude map and the residual amplitude map. All examples showed are for the frequency band from 0.065 to 0.11Hz.

# RESULTS

The main objective of this work is to assess the utility of amplitude information for surface waves. In other to do that, the amplitude-distance plots and spectral amplitude

maps were produced and analyzed. Here we aim to get and describe as much information as possible from these results.

## Amplitude-Distance Plots

The amplitude-distance plots were produced considering the amplitude behavior observed in the data for one earthquake at the time, therefore, it is possible to observe the amplitude decay for only one area of the United States in one plot. Figure 15 shows the amplitude-distance plot for the earthquake of 2013, when most of the TA stations were placed in eastern of the United States.

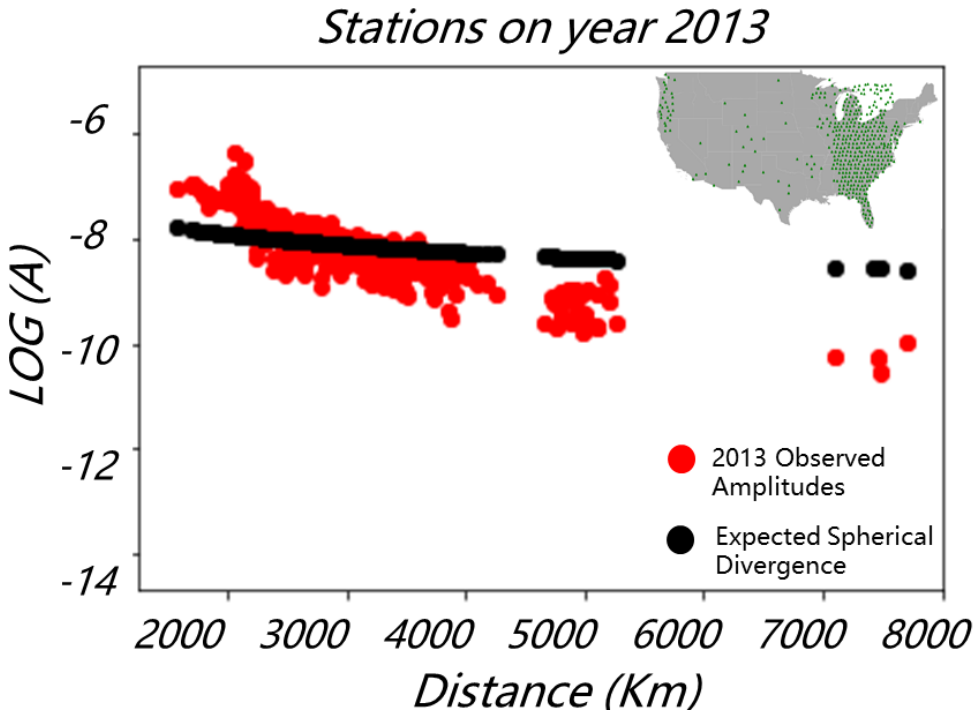


Figure 15 – Red dots show observed amplitudes recorded by stations set along year of 2013. Black dots represent the expected behavior of amplitude changing when considering geometrical spreading phenomenon.

On Figure 15 the amplitude decays with distance, as expected, however, looking at the expected circular divergence curve, it shows that this phenomenon is insufficient to explain the amplitude decay observed on the data. When the effect of frictional attenuation is included (figure 16), the prediction more accurately matches the observed data, giving a reasonable explanation for the amplitude decay observed in the data.

By repeating the process for all of the earthquakes, the degree to which the amplitude variation with distance for different regions of the United States can be measured. On figure 17, this behavior is presented in amplitude-distance plots for two distinct geologies, the eastern and western of the United States. When looking at the amplitude behavior with distance, different locations present different decays. For instance, it was possible to

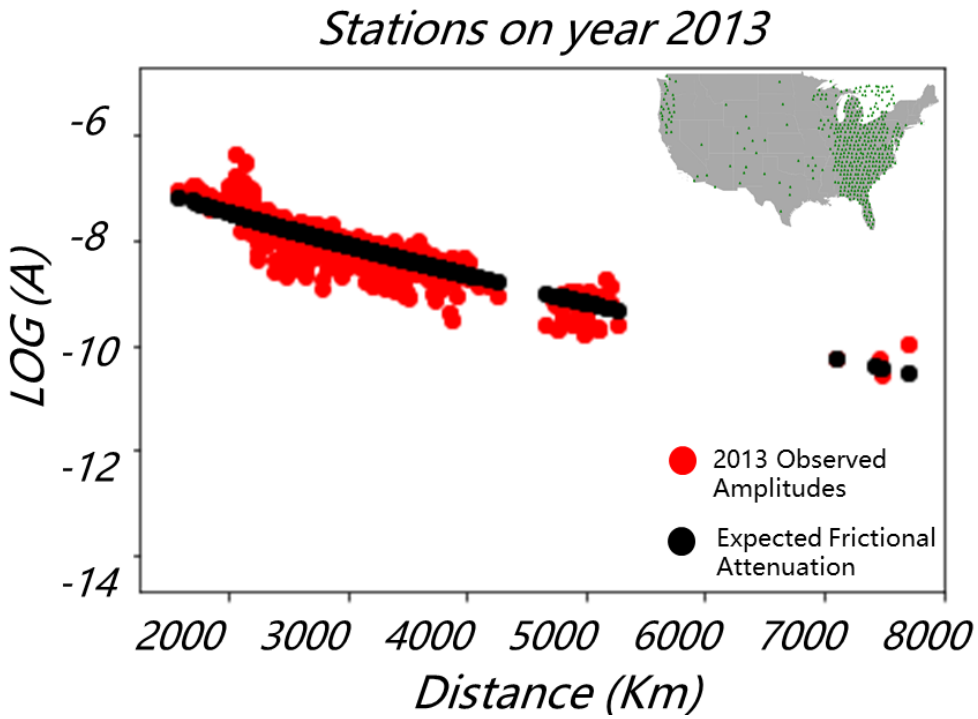


Figure 16 – Red dots show observed amplitudes recorded by stations set along year of 2013. Black dots represent the expected behavior of amplitude changing when considering both geometrical spreading and attenuation phenomena.

infer different attenuation coefficients and Q factors for both curves using the equations 3.2 and 3.3. It was found Q factors of 243 and 170 for eastern and western of the country, respectively, which means more attenuation for western of the United States.

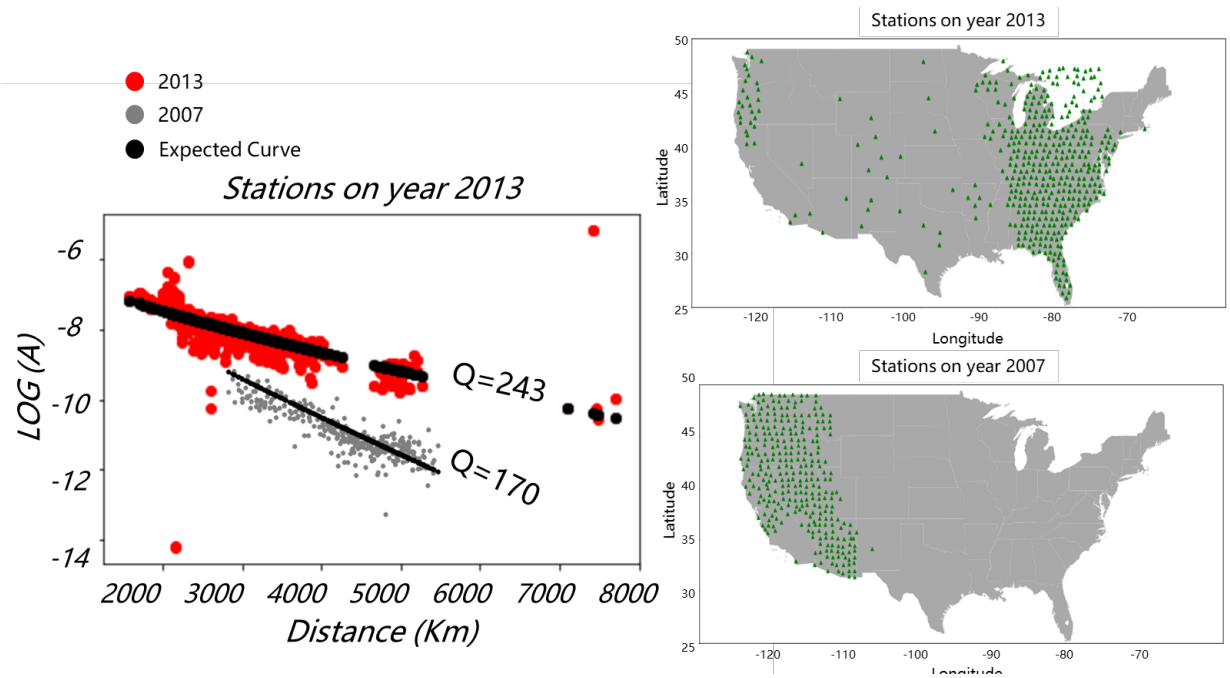


Figure 17 – The plot shows the amplitude-distance behavior for two different locations of the United States. These decays allow to infer different Q factors for the curves.

## Attenuation Maps

The amplitude-distance plots were reasonably consistent along the United States. For sets of stations crossing areas with distinct attenuation level, it was possible to observe different trend lines on the plots (Figure 18). This allowed us to estimate different Q factor for the same set of stations. On figure 18, it is clear that a single trend line cannot approximate all the stations on the plot. The stations with range smaller than 2250 km show a much faster decrease of amplitude than the more distant stations, which indicates higher attenuation (lower Q) at the shorter distances. The lower Q stations are on the periphery of the Gulf of Mexico, whereas the more distant, higher Q are on the North American craton.

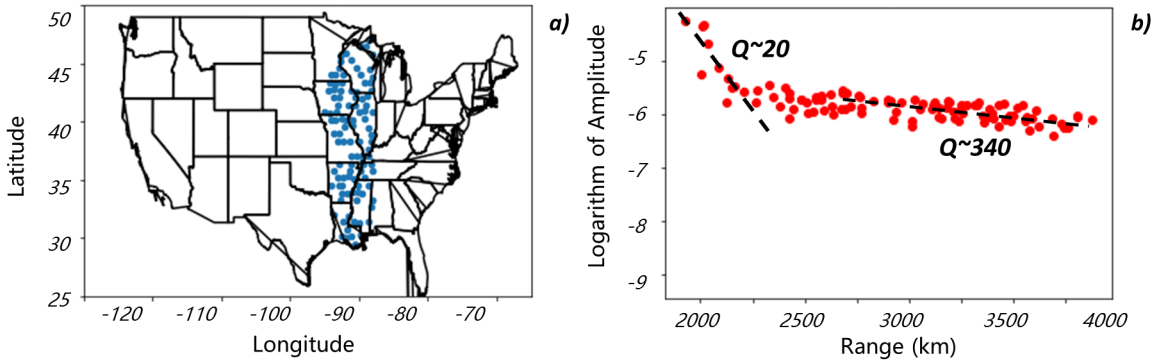


Figure 18 – Location of set of stations for transportable array in 2012 used for computing Q factor. b) Logarithm of the spectral amplitude (10s of period) plot, showing different behavior for ranges greater than 2250km. For stations closer to the source the estimated Q was about 20, meanwhile the others had an estimated Q of 340.

The quantity $Q^{-1}$ is more meaningful than is $Q$, because it is more closely related to the decay rate (see Equation 3.3). The consistency of the amplitude-range plots allowed computing $Q^{-1}$ maps for all the transportable array stations and all period ranges used in this study (Figure 19). Overall, it is possible to observe some consistency among the inverse of Q maps for different frequencies. In all maps, this is present on features in Arizona (feature 1), south Texas, Louisiana and sometimes extending south to Florida (feature 2).

## Spectral Residual Amplitude Maps

The spectral residual amplitude maps were produced for the different frequency ranges were computed. Different maps for different central periods of 20, 10, 7 and 5 seconds are showed on figures 20 parts a), b), c) and d), respectively. The longer period bands sense more deeply in the Earth than do the shorter ones. The uppermost mantle is

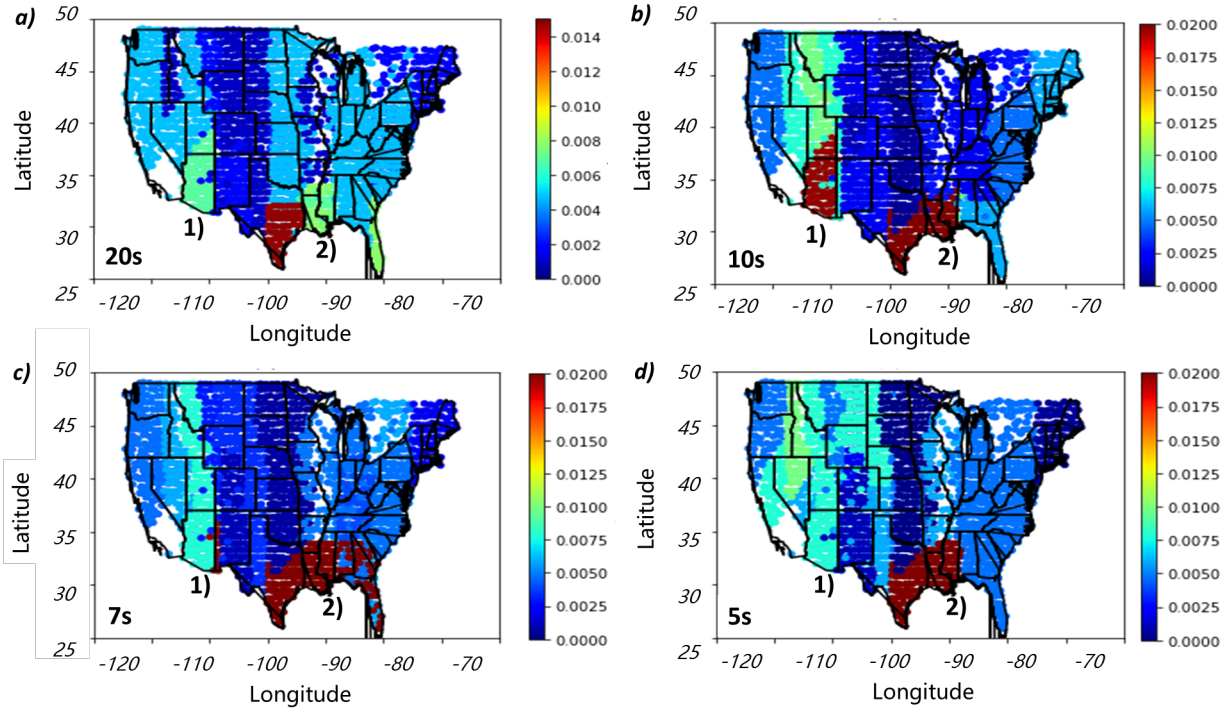


Figure 19 – : $Q^{-1}$ maps computed for the whole United states using amplitude information from surface waves. (a) 20 s period. (b) 10 s. (c) 7s. (d) 5 s. Two features with high attenuation are denoted 1) and 2).

sampled by the 20 s period data; the upper crust by the 5s period data. From figure 20, it is very clear there is coherent structure on the amplitude maps.

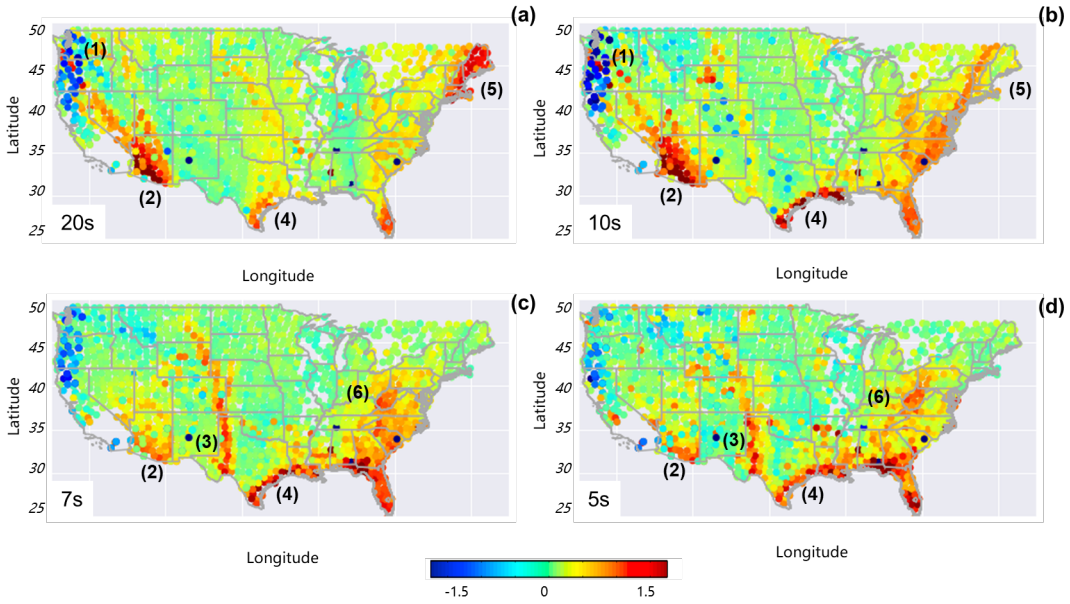


Figure 20 – Parts a, b, c and d show the spectral residual amplitude maps for central period of 20,10,7 and 5 seconds, respectively. Warmer colors represent higher residual amplitudes. Some important features observed in the maps are numbered from 1 to 6.

In all maps, it is possible to observe a negative feature nearby western Washington-Oregon (feature 1). For longer periods the negative feature is stronger and stretches down to north California. It is also possible to see a strong positive amplitude linear structure in Arizona (feature 2). For higher periods, the positive amplitude feature is stronger and thicker. In addition, for shorter periods (5-7s), we see a strong positive feature that trends in approximately the south-north direction (feature 3). In south Texas, we observe a strong positive feature that is parallel to the coastline (feature 4). In the shorter period maps (5-7s) this feature stretches from Louisiana to Florida, but at longer periods, it is less continuous. The central part of the US (between Mississippi river and the Appalachians) has relatively low amplitude except for some features, such as a strong positive feature trend in the northeast of United States (feature 5), observed clearer on the higher period maps. On the eastern it is also observed some high amplitude blobs (feature 6), mainly on smaller period maps.

# DISCUSSIONS

The amplitude spectral maps and the inverse of Q maps computed in this work show high level of consistency. Figure 21 shows both maps for 10s period surface waves. The maps have similar features, such as the one on Arizona marked by the pink dashed line on figure 21a. This area with high attenuation matches the high amplitude anomaly observed on the spectral amplitude map. A white dashed line marks the second feature on 21a, which follows the coastline from Texas to Florida. This high attenuation feature matches with the black dashed line on 21b. Comparing these maps it is possible to relate high amplitude values with areas with high attenuation. This could lead to new possible interpretations of the spectral amplitude maps.

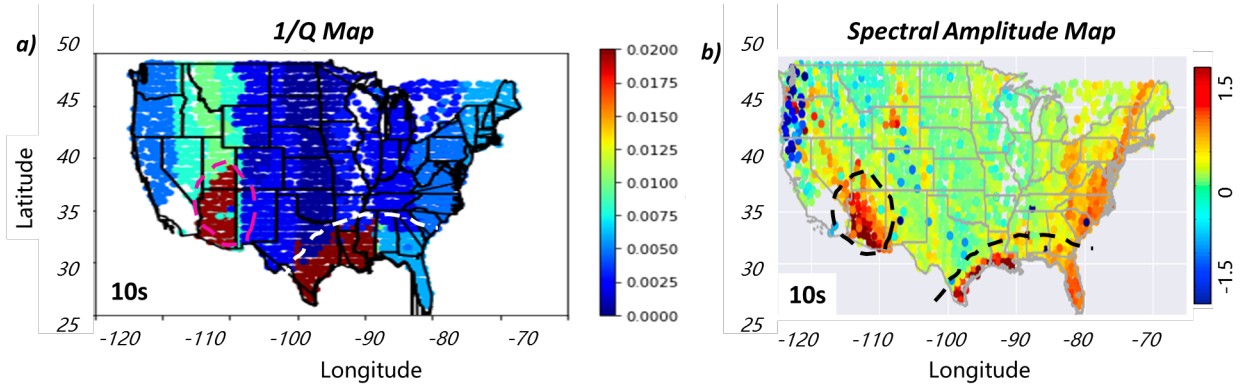


Figure 21 – a) shows the inverse of Q map for 10s period surface waves.b) shows the spectral amplitude map for 10s period surface waves. Hotter colors represent higher attenuation and higher amplitude, respectively.

The spectral residual amplitude maps computed in this work can be compared with other works such as the surface wave phase velocity maps from EKSTRöM (2017). The

spectral amplitude maps computed in this work have a promising number of similarities from the previous work. In figure 22 some of those features are pointed out.

For the 20s period maps (Fig. 22a and 22b) it is observed a clear linear anomaly (feature 1 and 3) with direction closely north south. Features 2 and 4 is also present in both maps. For the 10 seconds period maps (Fig. 22c and 22d) the features 2 and 4 turn into features 5 and 6, which are stronger and more continuous.

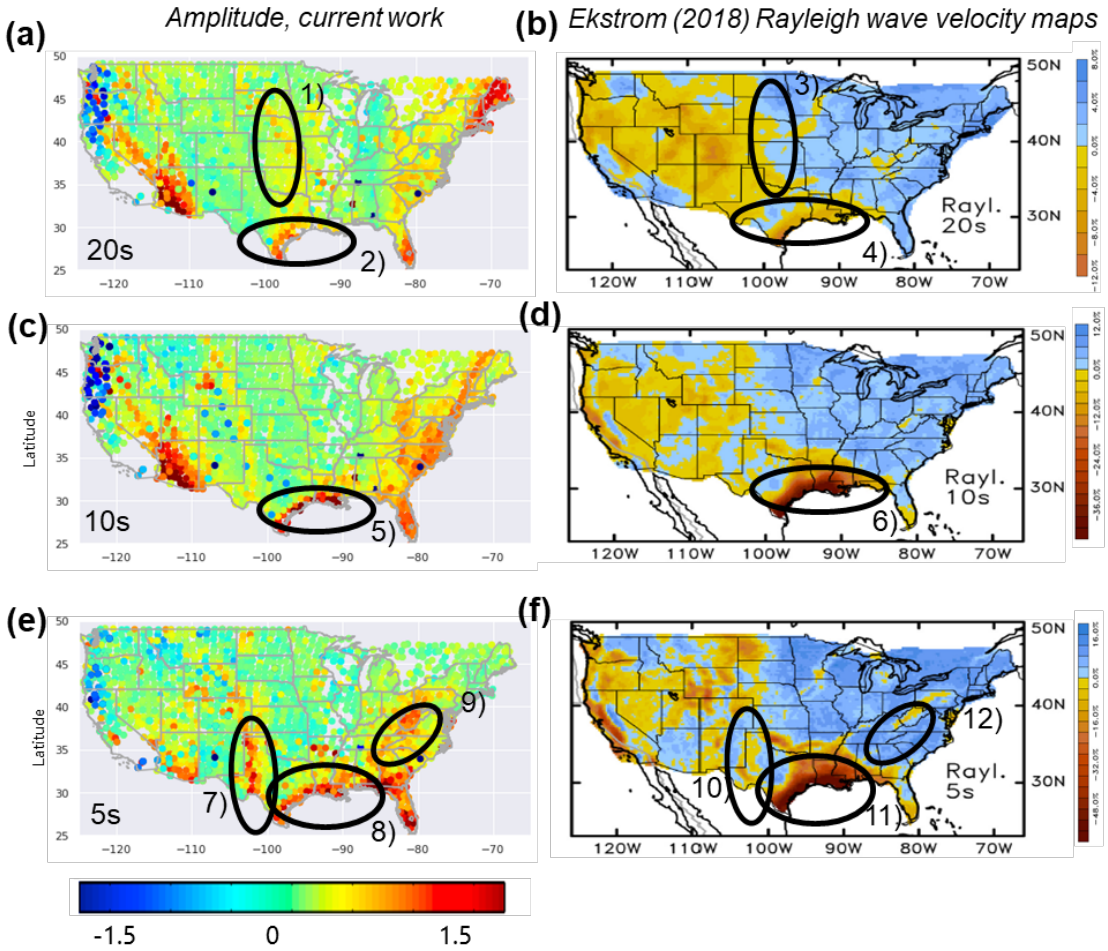


Figure 22 – Parts a) and b), c) and d) and e) and f) show the comparison between the computed spectral amplitude maps for 20,10 and 5 seconds, respectively, in respect to the velocity maps computed by EKSTRöM (2017).

Again, this observation is coherent for both amplitude and velocity maps. On the 5 seconds period maps (Fig. 22e and 22f) we see feature 7 and 10, closely north-south anomalies; features 8 and 11 stronger than 5 and 6 (Fig. 22c and 22d); and features 9 and 12, that seem to coincide with the Northern Appalachian anomaly described as a local mantle upwelling in previous works such as MENKE et al. (2016) and LOPES; MENKE (2017).

Figure 23 shows a comparison between the 20 seconds period amplitude map and SCHMANDT; LIN map for 200km depth shear wave velocity anomalies. One more time,

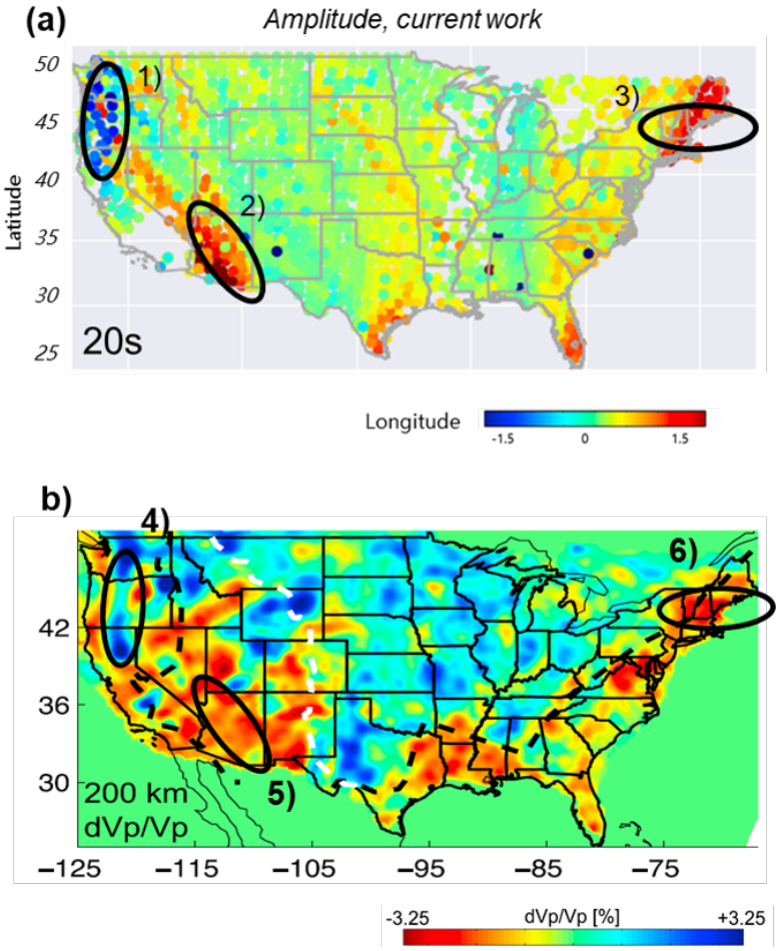


Figure 23 – Comparison between the 20 seconds period residual amplitude map (a) and the 200km depth shear wave velocity anomaly map (b) from SCHMANDT; LIN (2014. The black circles show some of the strong features present in both maps.

it is possible to observe plenty of similarities between the results. Figure 23 marks in black circles the common features in both maps, such as 1-4, 2-5 and 3-6. We can see that low velocity anomalies are related to higher amplitudes, such as described by the local energy conservation proposal described in equation 3.4.

In Texas and Louisiana the low amplitude anomalies observed in the maps (features 8 and 11 from Fig. 22e and 22f) are very well aligned with the gulf coastal plain and major geological features such as the Ouachita orogen and a complex fault and fractures system compose by the Baulcones, Luling, Tauco and Mexia fault zones. The Ouachita and Balcones trend includes the Paleozoic lithofacies and overthrust sheets that separates the North American central stable region (Craton) and the downwarping Gulf of Mexico basin (CARAN; M.; TOMPHSON, 1982). This tectonic boundary has remained active through most of Phanerozoic time and has influenced deposition, deformation, and volcanism along the southern margin of the continental Craton (CARAN; M.; TOMPHSON, 1982). The Ouachita orogen is also marked by a thick marine carbonate sequence above

basal Cretaceous that covers most of the system in central Texas. The low amplitude anomalies extends along Louisiana, showing an alignment with the Wilcox Group strata, an important economic resource, containing important aquifers (THORKILDSEN; PRICE, 1991), significant percentage of Texas lignite coal reserves and important hydrocarbon targets in the northwestern Gulf of Mexico (MEYER et al., 2005).

This Gulf Coast is also the site of the Northern Gulf Anomaly (NGA), a region of usually hot temperatures (KRAUSS; MENKE, 2020), consistent with the high attenuation we observe in this region. However, the NGA is believed to be centered in the mid-asthenosphere at 200 km depth - a deeper depth than can be sensed by 20 s or shorter period waves. Consequently, we do not believe that our data is sensitive to it.

The low amplitude anomalies seen in the western coast of United States (features 2 and 5 from figure 22a and 22b) are mostly located in the state of Arizona and are very well aligned with the transition zone in central Arizona between the basin and range and Colorado Plateau. The Arizona state straddles two of the majors physiographic subdivisions in United States: The basin and range and Colorado plateau provinces (FENNEMAN, 1928). The Transition Zone corresponds to the location of a substantial change in crustal thickness and related change in the Bouguer gravity in Arizona. The crust is about 25-30 km thick under the Basin and Range of west central Arizona. Crustal thickness in the southern Colorado Plateau is approximately 40 km. This 10-15 km increase in crustal thickness occurs across a horizontal distance of about 100km in the region of the Transition Zone and adjacent Basin and Range. Heat flow and the corresponding Curie point depths also show large change from the Basin and Range to the Colorado Plateau. Relative to the Colorado Plateau, the heat flow and Curie point in the Basin and Range are considered high and shallow.

There are also recent works on surface waves records that we could compare the results with. MAGRINI et al. (2021) used cross-correlate ambient seismic signal to compute 3–15 s period range phase velocity maps. Figure 24 shows a comparison between MAGRINI et al. phase velocity results and the residual spectral amplitude map for 5s period Rayleigh waves. The black dashed lines mark the main common features between the two maps. The positive amplitude anomalies in west and south Texas show in phase velocity map as low velocity zones. In eastern United States the negative amplitude anomaly matches in direction with the low velocity trend in the phase velocity map. These common features are consistent with results from EKSTRöM (2017) as well.

Generally speaking, high amplitude features in our maps correlate with slow features in other authors phase velocity maps and low amplitude features correlate with fast region. The sign of this correlation rules out the possibility that we are detecting local variations in frictional attenuation, because low velocity and high attenuation typically correlate because are caused by high temperature. This leaves lensing and local conservation of

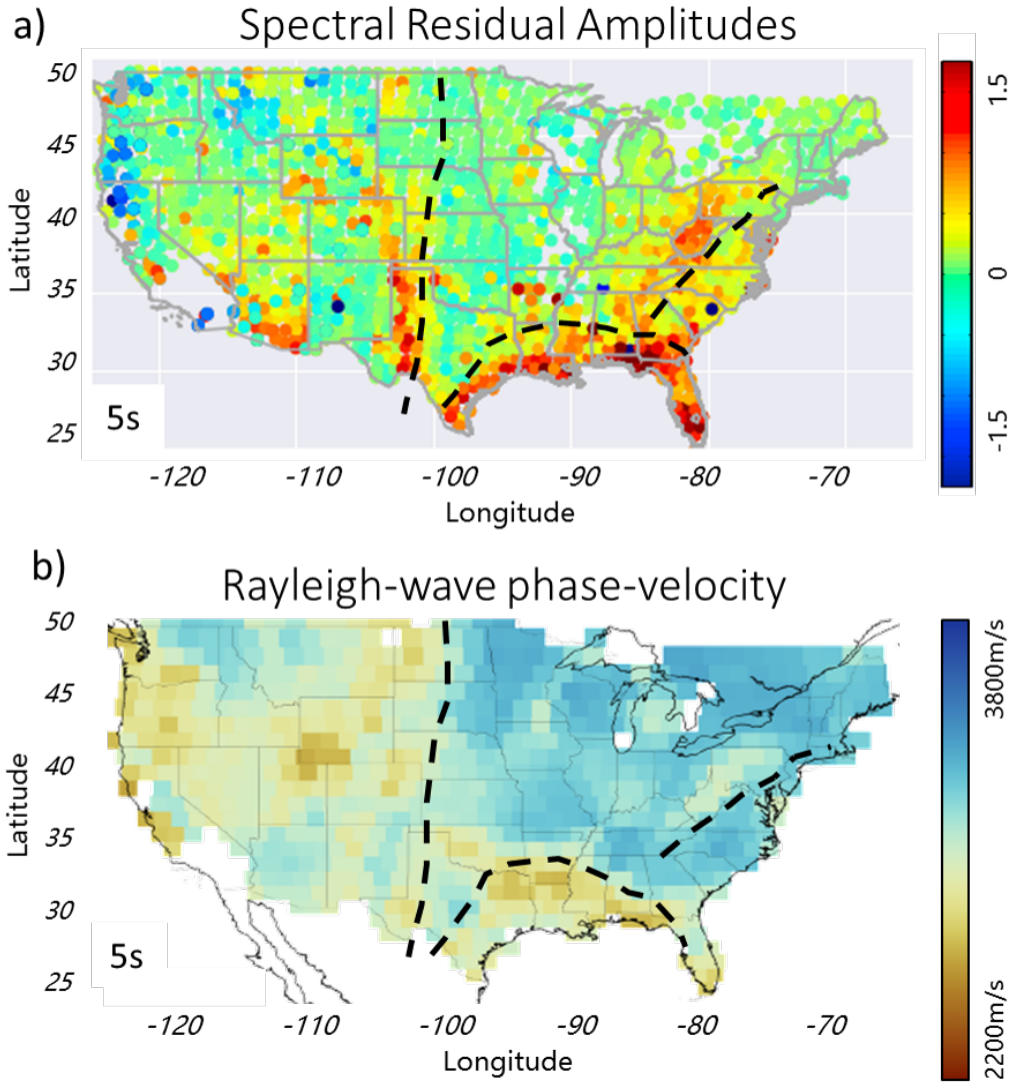


Figure 24 – Comparison between the 5 seconds period residual amplitude map (a) and the 5s period Rayleigh wave phase velocity map (b) from MAGRINI et al. (2021. The black dashed lines mark the main common features in both maps.

energy as possible causative mechanisms, as both are consistent with a negative correlation. Focusing could conceivably play a role in the high amplitudes at the Northern Appalachian Anomaly in New England, for it is has roughly circular shape that might cause strong lensing. However, the shape of other anomalies is less favorable for lensing. For instance, a linear-shaped anomaly, such as the one in the Pacific Northwest ought to have no focusing at all. Thus, we believe that local conservation of energy is the more plausible mechanism; that is, the amplitude anomalies reflect local changes in the phase velocity of the Rayleigh waves.

Figure 25 compares two different profiles. The left profiles represent seismic velocities and the right ones Rayleigh waves amplitudes. The black lines are reference profiles and the

red lines are profiles when disturbing the seismic velocities in about 10%. The perturbation on the Rayleigh waves amplitudes are proportional to the changes in the seismic velocities, therefore, this 10% change in velocity leads to a 10% change in the amplitude (equation 3.4). However, when observing the residual spectral amplitude maps we see the amplitudes are varying from 60% below average to 170% above average, much more than the possible velocity change expected in the Earth's crust. These amplitude variations are not well explained by the local energy conservation equations what could lead us to interpret that we are experiencing significant conversion to higher modes.

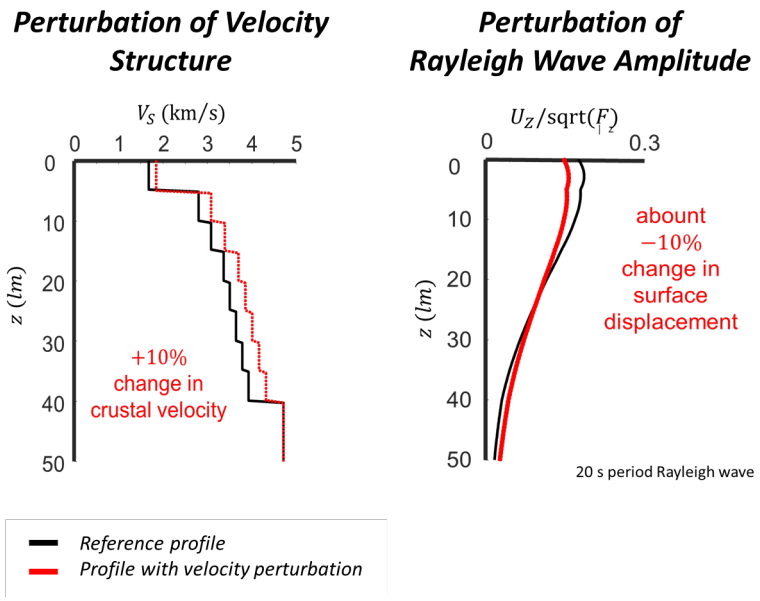


Figure 25 – Expected variation in surface waves amplitudes for a 20 seconds period Rayleigh wave.

# CONCLUSIONS

A Python-based data analysis procedure was developed to retrieve, process and analyze earthquake seismic data from IRIS database in order to extract precise estimates of Rayleigh seismic wave amplitudes in a suite of period bands ranging from 20 to 5 s. These amplitude estimates were analyzed in two different ways: (1) To infer seismic attenuation in different geographical regions using their decay with distance, and to interpret these broad patterns in terms of geology; and (2) to image the United States using spectral amplitudes residuals; that is, the deviation above and below that expected from circular divergence and Q, and to relate imaged structures to previously published maps of phase velocity. As expected on the basis of previous studies, the regionally-averaged Q was found to be low in the Basin and Range province of western United States and especially in Arizona, and less expected, along the US Gulf Coast and (for the longer periods only) in Florida.

The spectral residual amplitude maps showed significant geographical coherency, with many features ranging from hundreds to thousands of km in size. Many of these features, such as those in the Pacific Northwest, Arizona and New England, correlated well with features in phase velocity maps from previous works. Others, such as the one om Florida, do not appear in these other maps and warrant further investigation.

One other interesting conclusion from this work is that we could produce high quality maps using only one earthquake per location. This could lead to spotting smaller crust features that would be washed out by methods that average many earthquakes. Besides that, it would be possible to compare amplitude maps from earthquakes from different directions and spot important differences.

Another important impression is the unexpected behavior of surface waves amplitudes when it comes to the variation considerably large.. This could point that some aspect of the propagation of surface waves is not fully understood. One possibility is that surface waves are coupling into body waves, what could be more explored in future studies.

Overall, this study indicates that spectral amplitude residual maps potentially are a source of information about Earth structure that compliments traditional phase velocity maps.

## AKNOWLEDGEMENTS

The authors would like to thank to IRIS Data Services and US Geological Survey for providing data needed for this research.

# References

ABBOTT, D.; MOONEY, W. The structural and geochemical evolution of the continental crust: Support for the oceanic plateau model of continental growth. *Reviews of Geophysics*, v. 33, n. S1, p. 231–242, 1995. Disponível em: <https://agupubs.onlinelibrary.wiley.com/doi/abs/10.1029/95RG00551>.

ARNDT WALTER J. BAWIEC, S. R. E. Geology of the conterminous United States at 1:2,500,000 scale; a digital representation of the 1974 P.B. King and H.M. Beikman map. *U.S. Geological Survey*, 1994. Disponível em: <https://doi.org/10.1111/j.1365-246X.1979.tb04790.x>.

CARAN, S. C.; M., W. C.; TOMPHSON, E. J. Lineament analysis and inference of geologic structure : examples from the balcones ouachita trend of texas. *UT Libraries*, 1982. Disponível em: <https://repositories.lib.utexas.edu/bitstream/handle/2152/78047/txu-oclc-8419693.pdf?sequence=1&isAllowed=y>.

COUCH, R. W.; RIDDIHOUGH, R. P. Chapter 8: The crustal structure of the western continental margin of North America. In: *Geophysical Framework of the Continental United States*. Geological Society of America, 1989. ISBN 9780813711720. Disponível em: <https://doi.org/10.1130/MEM172-p103>.

DZIEWONSKI, A. M.; ANDERSON, D. L. Preliminary reference earth model. *Physics of the Earth and Planetary Interiors*, v. 25, n. 4, p. 297–356, 1981. ISSN 0031-9201. Disponível em: <https://www.sciencedirect.com/science/article/pii/0031920181900467>.

EKSTRöM, G. Short-period surface-wave phase velocities across the conterminous united states. *Physics of the Earth and Planetary Interiors*, v. 270, p. 168–175, 2017. ISSN 0031-9201. Disponível em: <https://www.sciencedirect.com/science/article/pii/S0031920117301942>.

FENNEMAN, N. M. Physiographic divisions of the united states. *Annals of the Association of American Geographers*, Taylor & Francis, v. 18, n. 4, p. 261–353, 1928.

FREI, L. S. Additional paleomagnetic results from the Sierra Nevada: Further constraints on Basin and Range extension and northward displacement in the western United States. *GSA Bulletin*, v. 97, n. 7, p. 840–849, 07 1986. ISSN 0016-7606. Disponível em: <https://doi.org/10.1130/0016-7606(1986)97<840:APRFTS>2.0.CO;2>.

GANS, P. B.; BOHRSON, W. A. Suppression of volcanism during rapid extension in the basin and range province, united states. *Science*, v. 279, n. 5347, p. 66–68, 1998. Disponível em: <https://www.science.org/doi/abs/10.1126/science.279.5347.66>.

HACıEFENDIOğLU, K. et al. Multi-point response spectrum analysis of a historical bridge to blast ground motion. *Structural Engineering and Mechanics*, v. 53, p. 897–919, 03 2015.

HATCHER ROBERT D., J.; THOMAS, W. A.; VIELE, G. W. *The Appalachian-Ouachita Orogen in the United States*. Geological Society of America, 1989. ISBN 9780813754529. Disponível em: <https://doi.org/10.1130/DNAG-GNA-F2>.

HATCHER ROBERT D., T. W. A. V. G. W. *The Geology of North America*. 3. ed. [S.l.]: The Geological Society of America, 1989.

HOHENSINN, R. *Detection of Hazardous Ground Movements with Instantaneous Velocity Estimates by GNSS*. Tese (Doutorado), 06 2019.

J., S.; A., C.; E., R. Understanding the fundamentals of earthquake signal sensing networks. *Analog Dialogue*, v. 53, n. 3, 2019.

KRAUSS, Z.; MENKE, W. The northern gulf anomaly: P-and s-wave travel time delays illuminate a strong thermal feature beneath the northern gulf of mexico. *Earth and Planetary Science Letters*, Elsevier, v. 534, p. 116102, 2020.

KREEMER, C. Absolute plate motions constrained by shear wave splitting orientations with implications for hot spot motions and mantle flow. *Journal of Geophysical Research*, v. 114, 2009.

LAY, T.; WALLACE, T. Modern global seimology. In: _____. [S.l.: s.n.], 1995. v. 58.

LOPES, D.; MENKE, W. Full wavefield simulations in an anisotropic media applied to the study of the northern appalachian anomaly. Fifteenth International Congress of the Brazilian Geophysical Society. 2017. Disponível em: <https://sbgf.org.br/mysbgf/eventos/expanded_abstracts/15th_CISBGf/Full%20wavefield%20simulations%20in%20an%20anisotropic%20media%20applied%20to%20the%20study%20of%20the%20Northern%20Appalachian%20Anomaly.pdf>.

MAGRINI, F. et al. Rayleigh-wave attenuation across the conterminous united states in the microseism frequency band. *Scientific Reports*, v. 11, p. 10149, 05 2021.

MENKE, W. et al. The northern appalachian anomaly: A modern asthenospheric upwelling. *Geophysical Research Letters*, v. 43, n. 19, p. 10,173–10,179, 2016. Disponível em: <https://agupubs.onlinelibrary.wiley.com/doi/abs/10.1002/2016GL070918>.

MEYER, D. et al. Emergence of the lower tertiary wilcox trend in the deepwater gulf of mexico. *World Oil*, v. 226, p. 72–77, 05 2005.

PAKISER, L.; MOONEY, W. *Geophysical Framework of the Continental United States*. California, U.S.: Geological Society of America, 1989. v. 1.

ROMANOWICZ, B. A. Seismic structure of the upper mantle beneath the United States by three-dimensional inversion of body wave arrival times. *Geophysical Journal International*, v. 57, n. 2, p. 479–506, 05 1979. ISSN 0956-540X. Disponível em: <https://doi.org/10.1111/j.1365-246X.1979.tb04790.x>.

SCHMANDT, B.; LIN, F. P- and s-wave tomography of the mantle beneath the united states. *Geophysical Research Letters*, v. 41, 09 2014.

SHEARER, P. M. *Introduction to Seismology*. 3. ed. [S.l.]: Cambridge University Press, 2019.

THORKILDSEN, D.; PRICE, R. Ground-water resources of the carrizo-wilcox aquifer in the central texas region. *Texas Water Development Board*, 1991. Disponível em: <https://agris.fao.org/agris-search/search.do?recordID=US9317547>.

WATTS, A. Unlocking the cascadia subduction zone's secrets: Peering into recent research and findings. *Earth Magazine*, 2014.